Biomolecules & Biomedicine

RESEARCH ARTICLE

# LNK expression, subcellular localization and survival associations in breast, cervical and colorectal cancer

Jessica C. Mantilla-Ollarves[1,2], Alejandro Sánchez-Carballido[1,2], Alejandro Ordaz-Ramos[3], Cecilia Aguilar[1], Miguel Tapia-Rodríguez[4], Liliana Cortés-Ballinas[1], Laura Velázquez[5], and Leticia Rocha-Zavaleta[1,6*]

**The role of lymphocyte adaptor protein (LNK) in breast, cervical and colorectal cancer remains incompletely characterized. We examined LNK expression, subcellular localization and associations with survival across these cancers. Gene Expression Profiling Interactive Analysis and cBioPortal were used to assess *LNK* messenger ribonucleic acid (mRNA) expression, while Kaplan–Meier Plotter was used for exploratory survival analyses. Western blotting and quantitative confocal immunofluorescence assessed protein expression and localization in 12 cancer cell lines and three non-tumoral controls. *LNK* mRNA expression varied among tumor subtypes and was significantly lower in cervical tumors than in adjacent normal tissue. Higher expression was associated with longer overall and recurrence-free survival in triple-negative breast cancer but shorter survival for both endpoints in colorectal cancer; no significant associations were observed in cervical cancer. LNK was detected in the nucleus and cytoplasm of all cancer cell lines. Significant nuclear predominance was observed in one of four triple-negative breast cancer cell lines and three of four cervical cancer cell lines, whereas their non-tumoral controls showed cytoplasmic predominance. Colorectal cancer cell lines displayed heterogeneous subcellular distributions. These exploratory findings suggest cancer type-specific associations between LNK expression and survival that require independent validation, while nuclear localization warrants investigation of potential nuclear functions.**

Keywords: LNK, overall survival, recurrence-free survival, breast cancer, cervical cancer, colorectal cancer, subcellular localization.

## Introduction

Breast cancer (BC) is the most common cancer among females globally. Colorectal cancer (CRC) ranks third in new cases across both sexes worldwide. In low and middle Human Development Index countries, cervical cancer (CC) is the second most frequently diagnosed cancer. Furthermore, CRC is the second deadliest cancer globally, while BC and CC are the first and fourth leading causes of cancer-related mortality in women, respectively [1].

While BC, CC, and CRC have distinct etiologies, risk factors, and treatments [2–4], they share common alterations in key signaling pathways. These include the Janus kinase (JAK)-signal transducer and activator of transcription (STAT), phosphatidylinositol 3-kinase (PI3K)-protein kinase B (AKT), and mitogen-activated protein kinase (MAPK) cascades. Such alterations are linked to cell proliferation, migration, and chemoresistance in BC (particularly the triple-negative subtype, which lacks hormone receptor and human epidermal growth factor receptor 2 [HER2] expression) [5, 6], CRC [7–10], and CC [11–15]. Natural inhibitors, such as lymphocyte adaptor protein (LNK), can negatively regulate these molecular axes [16, 17].

LNK, a member of the SH2B adaptor protein family, possesses three functional domains: a carboxy-terminal SH2 region for target protein binding, an amino-terminal domain capable of homo- and heterodimerization with other SH2B family members, and a central pleckstrin homology (PH) domain [18] that interacts with phosphatidylinositol lipids in the cell membrane. Upon JAK-STAT pathway activation, LNK translocates to the inner membrane surface [19]. Here, it binds to phosphorylated JAK proteins via its SH2 domain, thereby inhibiting JAK kinase activity and blocking STAT transcription factor activation [20]. This action effectively interrupts downstream signaling. Evidence suggests that LNK also mediates the inhibition of PI3K-AKT and MAPK cascades, although the exact mechanism remains unknown. Given that JAK2 can activate both cascades, it is proposed that LNK indirectly regulates these pathways by blocking JAK2 activity [21].

[1]Departamento de Biología Molecular y Biotecnología, Instituto de Investigaciones Biomédicas, Universidad Nacional Autónoma de México, Mexico City, Mexico; [2]Programa de Doctorado en Ciencias Bioquímicas, Universidad Nacional Autónoma de México, Mexico City, Mexico; [3]Departamento de Medicina Genómica y Toxicología Ambiental, Instituto de Investigaciones Biomédicas, Universidad Nacional Autónoma de México, Mexico City, Mexico; [4]Unidad de Microscopía, Instituto de Investigaciones Biomédicas, Universidad Nacional Autónoma de México, Mexico City, Mexico; [5]Inserm UMR 1342, Institut de Recherche Saint-Louis, Hôpital Saint-Louis, Paris, France; [6]Programa Institucional de Cáncer de Mama, Instituto de Investigaciones Biomédicas, Universidad Nacional Autónoma de México, Mexico City, Mexico.

*Correspondence to Leticia Rocha-Zavaleta: lrochaz@iibiomedicas.unam.mx

DOI: 10.17305/bb.2026.14287

© 2026 Mantilla-Ollarves et al. This article is available under a Creative Commons License (Attribution 4.0 International, as described at https://creativecommons.org/licenses/by/4.0/).

Despite LNK's clear potential as a negative regulator in cancer, its role in solid tumors is poorly understood. Moreover, LNK expression has been studied in only a limited number of tumor types. For example, Lv and colleagues [22] evaluated LNK expression via immunohistochemistry in a very small sample of BC tumors ($n = 8$). They observed stronger immunostaining intensity in triple-negative BC samples compared to non-triple-negative samples. However, their study lacked analysis of normal breast tissue, rendering the results inconclusive and highlighting the need for further investigation into the potential significance of LNK expression in BC. Additionally, LNK overexpression has been detected in ovarian cancer [23], anaplastic thyroid carcinoma [24], glioblastoma [25], and melanoma [26], with all cases associating LNK overexpression with increased cell proliferation. In contrast, low LNK expression has been reported in CRC [27] and lung cancer [28], where it acts as a negative regulator of migration and invasion. Unfortunately, LNK expression has not been evaluated in CC. Similarly, there is a lack of studies assessing potential associations between LNK expression and clinical responses in patients diagnosed with BC, CC, and CRC.

For LNK to function as a negative regulator, it is hypothesized that it must translocate to the cell membrane to interact with target molecules. However, studies on the intracellular localization of LNK in solid tumors are very limited [23, 25]. In fact, LNK localization in BC, CC, and CRC cells remains unknown.

This study aimed to investigate LNK expression levels in BC, CC, and CRC. We also examined the protein's intracellular localization in cell lines derived from BC, CC, CRC, and non-tumoral control cells. Furthermore, we analyzed public datasets to explore the relationship between LNK expression and clinical outcomes in patients with BC, CC, and CRC. The findings are expected to provide insights into the potential association of LNK with BC, CC, and CRC and to contribute experimental data that may guide future investigations into the mechanistic roles of LNK in these tumor types.

## Materials and methods

### Cell lines

This study utilized the following CC cell lines: HeLa (ATCC CCL-2™), Ms751 (ATCC HTB-34™), and SiHa (ATCC HTB-35™), obtained from the American Type Culture Collection (ATCC, Rockville, MD, USA), and RoVa (donated by Dr. Alberto Monroy-García, UNAM, Mexico) [29]. The immortalized human keratinocyte cell line HaCaT served as a non-tumoral control. These cell lines were maintained in Roswell Park Memorial Institute (RPMI)-1640 medium with L-Glutamine (Biowest SAS). CRC cell lines HCT116 (ATCC CCL-247™), RKO (ATCC CRL-2577™), SW480 (CCL-228™), and SW620 (ATCC CCL-227™), along with the immortalized non-tumoral colon fibroblast cell line 112CoN (ATCC CRL-1541™) as a control, were maintained in Dulbecco's Modified Eagle Medium (DMEM) High Glucose w/ L-Glutamine (Biowest). Cells were grown in the appropriate medium supplemented with 10% Fetal Bovine Serum (FBS) (Biowest), penicillin, streptomycin, and amphotericin B (Cat. L0010, Biowest). The following BC cell lines were included: HCC1806 (ATCC CRL-2335™), HCC1937 (ATCC CRL-2336™), MDA-MB-231 (ATCC HTB-26™), and MDA-MB-468 (ATCC HTB-132™). These BC cell lines, also obtained from ATCC, were maintained in RPMI-1640 medium with L-glutamine, supplemented with 8% FBS, penicillin, streptomycin, and amphotericin B. The immortalized breast cell line MCF-10A (ATCC CRL-10317™), used as a non-tumoral control, was cultured in Procell System MCF10A Cell Complete Medium (CM-0525, Procell Biotechnology, Singapore, Pte. Ltd.). All cells were incubated at 37 °C in a humidified atmosphere with 5% $CO_2$ and used at low passages (5–30). Mycoplasma testing was performed by direct 4′,6-diamidino-2-phenylindole (DAPI)-DNA fluorescent staining. The identity of all cell lines was authenticated by Short Tandem Repeat (STR) profiling using the Cellosaurus STR similarity search tool at the Genomic Diagnostic Laboratory (Instituto Nacional de Medicina Genómica, Mexico City, Mexico).

### Western blot

Total protein extracts were prepared using radioimmunoprecipitation assay (RIPA) buffer (150 mM NaCl, 50 mM Tris-HCl, 1% NP40, 0.5% sodium deoxycholate, 0.1% sodium dodecyl sulfate [SDS]) supplemented with 1× phosphatase inhibitor cocktail (Sigma-Aldrich, St. Louis, MO, USA) and 1× protease inhibitor cocktail (cOmplete Tablets Mini EASYpack; Roche Diagnostics GmbH.; Mannheim, Germany). Protein concentration was quantified using a detergent compatible (DC) protein assay kit (Bio-Rad Laboratories Inc.; Hercules, CA, USA). Proteins (30 μg of each extract) were separated on a 10% sodium dodecyl sulfate–polyacrylamide gel electrophoresis (SDS-PAGE) gel and then transferred to polyvinylidene fluoride membranes (Merck Millipore Ltd., Tullagreen, Carrigtohill, Ireland). Membranes were blocked with 5% non-fat milk in Tris-buffered saline (TBS) and subsequently incubated overnight at 4 °C with anti-LNK (Cat. sc-393709; Santa Cruz Biotechnology Inc., Santa Cruz, CA, USA) and anti-glyceraldehyde-3-phosphate dehydrogenase (GAPDH) (Cat. GTX100118; GeneTex, Inc., Irvine, CA, USA) primary antibodies, diluted 1:1000 and 1:5000, respectively, in 5% non-fat milk in TBS. Following primary antibody incubation, membranes were incubated with horseradish peroxidase-conjugated secondary antibodies: anti-rabbit immunoglobulin G (IgG) (Cat. GTX213110-01, GeneTex) and anti-mouse (Cat. GTX77315, GeneTex), both diluted 1:10,000 in 5% non-fat milk in TBS. Specific protein bands were detected using chemiluminescence with SuperSignal West Femto Maximum Sensitivity Substrate (Thermo Scientific Co., Waltham, MA, USA). Densitometric analysis was performed using Fiji software [30]. Band intensity was quantified by generating an intensity plot for each protein band and calculating the area under the curve. The integrated density values for LNK were normalized to the respective GAPDH loading controls. Relative protein expression levels were calculated as fold change values relative to the non-tumoral control cell line.

### Confocal microscopy

Cells were seeded onto poly-L-lysine coated coverslips, then fixed with 2% paraformaldehyde and permeabilized with 0.05% Triton for 10 min. Following three washes with 0.1 M glycine in phosphate-buffered saline (PBS), cells were incubated in TBS for 15 min. After blocking for 1 hour with a solution containing 0.15 M bovine serum albumin, 10% FBS, and 0.3 M glycine in PBS/0.1% Tween, cells were incubated overnight with the primary anti-LNK antibody (Cat. sc-393709, Santa Cruz Biotechnology). Subsequently, cells were washed three times with PBS and incubated for 2 h at room temperature, protected from light, with the Alexa Fluor 555-conjugated anti-mouse secondary antibody (Cat. A31570, Invitrogen, Eugene, OR, USA). After three final PBS washes, cells were mounted in Vectashield Antifade Mounting Medium with DAPI (Vector Laboratories, Burlingame, CA, USA).

Confocal images were acquired using a Nikon A1R+ laser scanning confocal head coupled to an Eclipse Ti-E inverted microscope (Nikon Corporation, Tokyo, Japan). This system, located at the Unidad de Microscopia, Instituto de Investigaciones Biomédicas, UNAM (Research Resource Identifier [RRID]: SCR_022204), was equipped with a TI-S-E motorized stage (Nikon) and controlled by Nis Elements C v.5.20 software. Cells were analyzed with a Plan Apo VC 60X WI DIC N2 objective (N.A. 1.2). Single-plane images or z-stacks were sequentially captured using standard galvanometric scanners with excitation wavelengths of 405 nm (1.00 mW) and 561 nm (14 mW) via acousto-optic tunable filter (AOTF) modulation. The pinhole aperture was set at 26.82 μm, and emission light was detected by both standard and gallium arsenide phosphide (GaAsP) detectors. Images were then imported and visualized using Fiji [30].

### Quantitative analysis of immunofluorescence images and statistical analysis

Immunofluorescence was employed to determine the intracellular distribution of LNK in cell lines. From multiple confocal images across three independent experiments, 20 cells were randomly selected. Fluorescence intensity was quantified using Fiji [30]. Individual cells were manually segmented, and nuclear and cytoplasmic regions of interest (ROIs) were defined for each cell. Fluorescence intensity was measured as the mean gray value, representing the average pixel intensity within each ROI. Background intensity, determined from an empty field region, was subtracted from all ROI measurements.

Data were analyzed using Aligned Rank Transform (ART) to assess the effects of cell line and cellular compartment (nucleus vs cytoplasm). An ART analysis of variance (ANOVA) was performed to test main effects and interactions. Post hoc comparisons between the nucleus and cytoplasm were conducted using estimated marginal means from the ART model, aligned for the compartment effect, with Tukey adjustment for multiple testing. Statistical significance was set at $P < 0.01$. All statistical procedures were performed in RStudio (version 2023.03.1).

### Bioinformatic and statistical analyses

To evaluate *LNK* mRNA expression in tumor vs adjacent normal tissues, the Gene Expression Profiling Interactive Analysis (GEPIA) platform (https://gepia.cancer-pku.cn/) was utilized. GEPIA is a public web-based tool that integrates RNA sequencing data from The Cancer Genome Atlas (TCGA) and the Genotype-Tissue Expression projects, enabling comparative analyses between tumor and normal tissues through standardized processing pipelines [31]. Gene expression was analyzed in datasets from patients with BC, CRC, or CC. Expression levels were quantified using log2(TPM + 1) transformed values provided by the platform. Statistical comparisons between groups were performed using GEPIA's one-way ANOVA framework.

The association between *LNK* mRNA expression and clinical characteristics was investigated using data from the cBioPortal platform (https://www.cbioportal.org/). cBioPortal is a publicly available web resource that integrates multidimensional cancer genomics datasets, including TCGA and other studies, providing access to genomic, transcriptomic, and clinical information for large cancer cohorts. Expression and clinical data were obtained from the following TCGA cohorts: Breast Invasive Carcinoma (TCGA, PanCancer Atlas) for BC, Cervical Squamous Cell Carcinoma (TCGA, PanCancer Atlas) for CC, and Colorectal Adenocarcinoma (TCGA, PanCancer Atlas) for CRC [32]. Clinical data files (data_clinical_patient.txt and data_clinical_sample.txt) were matched to expression data (data_mrna_seq_v2_rsem_zscores_ref_all_samples.txt) using Sample ID. Relative gene expression levels (RNA-Seq by expectation-maximization data) were correlated with clinical characteristics such as molecular subtype, histological type, tumor stage, tumor–node–metastasis (TNM) classification, and tumor grade. Data distribution was assessed using a Shapiro–Wilk normality test. For comparisons between two groups, an unpaired *t*-test was used for parametric data, and a Mann–Whitney test for non-parametric data. For multiple comparisons, one-way ANOVA with a post hoc test was applied to parametric data, while the Kruskal–Wallis test was used for non-parametric data.

Survival analyses were conducted using the Kaplan–Meier Plotter (KMplot) online platform (https://kmplot.com/analysis/). KMplot is a public web-based tool for survival analysis, integrating gene expression data from multiple meta-analyses and clinical outcome data from various cancer cohorts, including TCGA, European Genome-phenome Archive, and Gene Expression Omnibus. This enables evaluation of associations between gene expression and patient survival [33–35]. RNA sequencing data was used for BC and CRC, while microarray (gene chip) data was used for CC. Patients were stratified using the platform's trichotomization setting, comparing the lowest quartile (Q1) against the highest quartile (Q4) of gene expression. Recurrence-free survival (RFS) and overall survival (OS) were the primary survival endpoints, with follow-up including all available time. Statistically significant differences between groups were analyzed using the univariate log-rank (Mantel–Cox) test. Hazard ratios and 95% confidence intervals were calculated using Cox regression models implemented in the platform. These survival studies were performed as exploratory analyses to assess the association between *LNK* mRNA expression and patient clinical outcomes across different cancer types and clinical endpoints. No correction for multiple comparisons was applied.

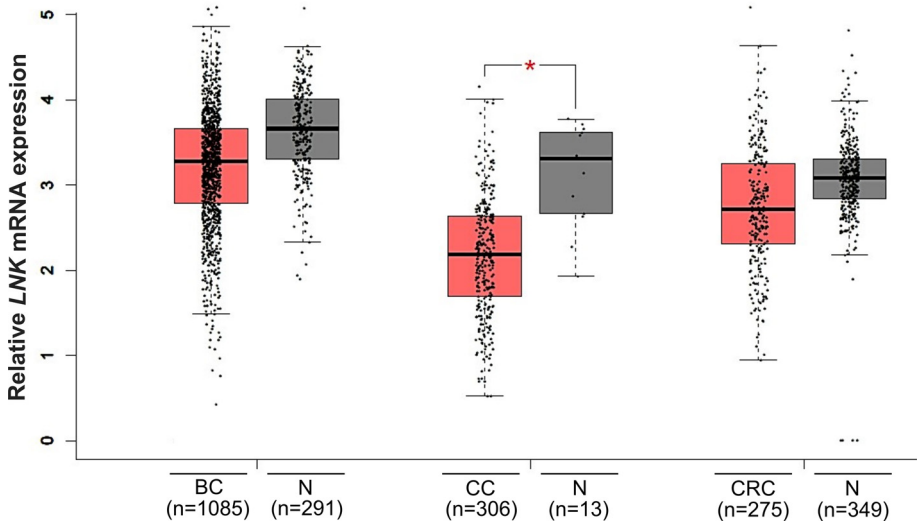



**Figure 1. *LNK* mRNA expression in BC, CC and CRC.** Relative *LNK* mRNA expression in tumor and N samples was analysed using GEPIA and is presented as $\log_2(\text{TPM} + 1)$. Tumor samples are shown in red and *N* samples in gray, with black dots representing individual samples. Sample sizes were 1,085 tumor and 291 N samples for BC, 306 tumor and 13 N samples for CC, and 275 tumor and 349 N samples for CRC. Differences between tumor and *N* groups were assessed using the one-way ANOVA framework implemented in GEPIA. *LNK* mRNA expression was significantly lower in CC tumors than in *N* samples, whereas the differences in BC and CRC were not statistically significant. * $P < 0.05$ for the indicated comparison. **Abbreviations**: ANOVA, analysis of variance; BC, breast cancer; CC, cervical cancer; CRC, colorectal cancer; GEPIA, Gene Expression Profiling Interactive Analysis; LNK, lymphocyte adaptor protein; mRNA, messenger ribonucleic acid; N, normal tissue; TPM, transcripts per million.

### Ethical statement

This study utilized publicly available datasets and did not require Institutional Review Board review.

## Results

### *LNK* mRNA expression in BC, CC and CRC tumors

The expression of LNK in BC, CC, and CRC tumors has not been extensively studied. Therefore, we initially interrogated public databases to assess *LNK* mRNA expression levels in BC, CC, CRC, and adjacent normal tissue samples. As depicted in Figure 1, *LNK* mRNA expression showed a non-significant trend to be lower in BC and CRC compared to adjacent normal tissue. However, for CC, statistical analysis revealed significantly lower *LNK* mRNA expression in tumor tissue than in adjacent normal tissue samples.

Given that cancer is now classified by both histological and molecular subtypes, we further evaluated *LNK* mRNA expression levels in samples categorized by tumor subtype to gain deeper insight into LNK expression in BC, CC, and CRC. For this analysis, BC data were collected from the TCGA PanCancer Atlas, where cohorts are classified by the PAM50 system into five molecular subtypes: luminal A, luminal B, normal-like, HER2-enriched, and basal-like (Figure 2A). The analysis demonstrated significant differences in *LNK* mRNA expression among BC subtypes; luminal A, luminal B, HER2-enriched, and basal-like subtypes exhibited significantly lower *LNK* mRNA expression compared to the normal-like subtype. Notably, *LNK* mRNA expression levels in basal-like samples were not significantly different from those detected in luminal A, luminal B, and HER2-enriched subtypes. Basal-like BC often overlaps with triple-negative BC, as this PAM50 subtype includes tumors expressing basal cell markers but lacking hormone and HER2 receptor expression. This aggressive BC subtype is of particular interest due to its association with faster tumor growth, metastasis, and high recurrence risk, with limited understanding of the molecules driving this behavior. Consequently, we focused our subsequent analysis on triple-negative BC.

CC cases were categorized into two prevalent histological subtypes: adenocarcinoma and squamous cell carcinoma (Figure 2B). Despite squamous cell carcinoma being more common than adenocarcinoma, statistical analysis revealed lower *LNK* mRNA expression in squamous cell tumors compared to adenocarcinomas. To substantiate this finding, further analysis included cells from both adenocarcinoma and squamous cell carcinoma types.

For CRC, analyzed cases were molecularly classified into chromosomal instability (CIN), genomically stable (GS), microsatellite instability (MSI), and DNA polymerase epsilon catalytic subunit (POLE) mutated categories. Significant differences in *LNK* mRNA expression were observed between CIN and MSI subtypes, as well as between GS and MSI subtypes (Figure 2C). These results suggest that among the more prevalent CRC subtypes (CIN, GS, and MSI), MSI tumors exhibit the highest *LNK* mRNA expression. To further explore this, we conducted *in vitro* analysis using CRC cell lines with and without MSI for comparison.

### Association of *LNK* mRNA expression with cancer progression

Our findings indicate that *LNK* mRNA expression levels can vary even among patients with the same tumor type. To determine if this molecule correlates with clinical indicators of disease progression, we stratified patients with triple-negative

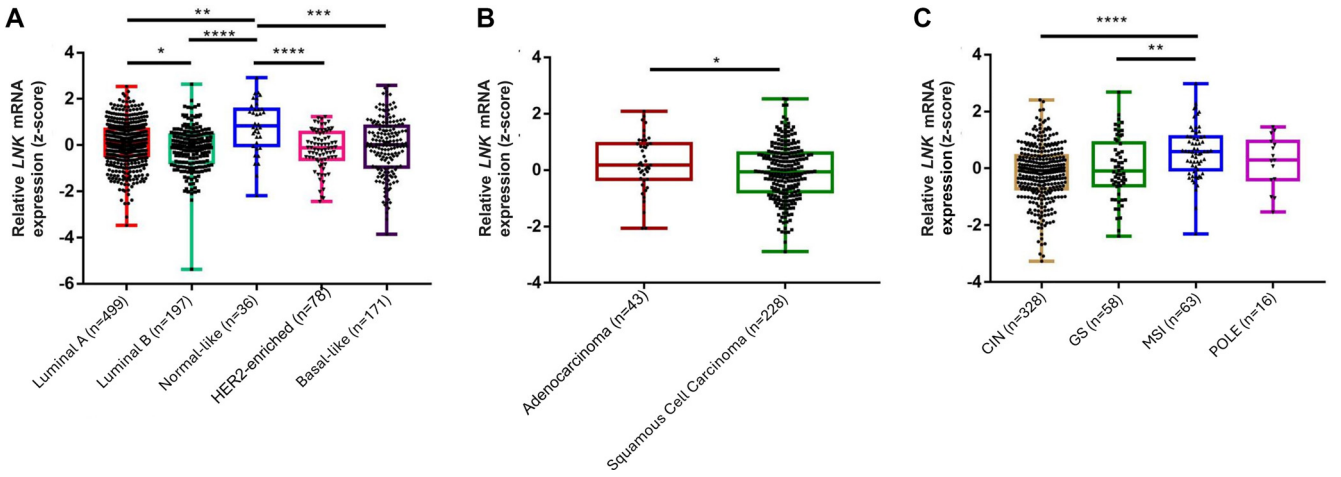



**Figure 2.** ***LNK*** **mRNA expression across molecular and histological subtypes of BC, CC and CRC.** Expression and clinical data were obtained from the TCGA PanCancer Atlas cohorts through cBioPortal and matched by sample identifier. Relative *LNK* mRNA expression is presented as z-scores. (A) BC samples classified by PAM50 subtype as luminal A, luminal B, normal-like, HER2-enriched or basal-like. (B) CC samples classified by histological subtype as adenocarcinoma or squamous cell carcinoma. (C) CRC samples classified by molecular subtype as CIN, GS, MSI or *POLE*-mutated. Black dots represent individual samples, and sample sizes are indicated in parentheses beneath each group. Two-group comparisons were performed using an unpaired *t*-test for parametric data or the Mann–Whitney test for non-parametric data. Comparisons among multiple groups were performed using one-way ANOVA with post hoc testing for parametric data or the Kruskal–Wallis test for non-parametric data. Horizontal bars indicate significant pairwise comparisons. * $P < 0.05$; ** $P < 0.01$; *** $P < 0.001$; **** $P < 0.0001$. **Abbreviations**: ANOVA, analysis of variance; BC, breast cancer; CC, cervical cancer; CIN, chromosomal instability; CRC, colorectal cancer; DNA, deoxyribonucleic acid; GS, genomically stable; HER2, human epidermal growth factor receptor 2; LNK, lymphocyte adaptor protein; mRNA, messenger ribonucleic acid; MSI, microsatellite instability; PAM50, prediction analysis of microarray 50; POLE, DNA polymerase epsilon; TCGA, The Cancer Genome Atlas.

BC, CC, or CRC by *LNK* mRNA expression level and analyzed OS and RFS as clinical endpoints.

As depicted in Figure 3A, triple-negative BC patients with high *LNK* mRNA expression demonstrated significantly longer OS than those with low expression. Conversely, CRC patients' OS was negatively correlated with *LNK* mRNA expression (Figure 3C). In CC cases, no correlation was found between OS and *LNK* mRNA expression (Figure 3B). Accordingly, RFS significantly correlated with higher *LNK* mRNA expression in triple-negative BC patients (Figure 3A). As anticipated, RFS in CRC patients was significantly lower when tumors expressed high *LNK* mRNA levels (Figure 3C). Finally, no correlation existed between *LNK* mRNA expression and RFS in CC patients (Figure 3B).

### Expression and subcellular localization of the LNK protein in cell lines

Exploratory analysis of datasets suggested that *LNK* mRNA expression and its potential association with clinical outcomes are tumor type-dependent. To expand on these observations, we evaluated LNK protein presence in triple-negative BC, CC, and CRC cell lines. We confirmed LNK expression in four triple-negative BC cell lines (HCC1806, HCC1937, MDA-MB-231, and MDA-MB-468), four CC cell lines (HeLa, Ms751, RoVa, and SiHa), and four CRC cell lines (HCT116, RKO, SW480, and SW620). Immortalized breast cells (MCF-10A), human keratinocytes (HaCaT), and colon fibroblasts (112CoN) were included as non-tumoral controls for BC, CC, and CRC, respectively. The main characteristics of each cell line are detailed in Table 1. Results showed LNK expression in all tested cell lines. While varying LNK levels were observed across cell lines, protein expression in cancer-derived cell lines tended to be higher than in their corresponding non-tumoral controls (Figure 4). This contrasts with patient data, where *LNK* mRNA expression tended to be higher in normal adjacent tissue than in tumor samples, though this difference was only significant in CC patients. Additionally, immortalized cells possess genetic changes not found in normal adjacent tissue, making immortalized cells and normal human tissue potentially non-comparable.

Given that amino acids in LNK's PH domain can interact with phosphatidylinositol lipids in the cell membrane, it has been proposed that this sequence enables LNK to translocate to the cell membrane, where active JAK molecules reside. Therefore, we next assessed LNK localization in cell lines via immunofluorescence.

Figure 5A displays microphotographs of four triple-negative BC cell lines. In all lines, LNK signals were detected in both the cell nucleus and cytoplasm. Quantitative analysis of LNK signal distribution showed predominant nuclear localization in the HCC1937 cell line. Although the nuclear LNK signal tended to be stronger than the cytoplasmic signal in HCC1806, MDA-MB-231, and MDA-MB-468 cells, the difference was not significant. Conversely, the LNK signal was significantly more intense in the cytoplasm than in the nucleus of non-tumoral MCF-10A control cells (Figure 5B).

Immunofluorescence staining of CC cell lines revealed that LNK is primarily localized in the cell nucleus in HeLa, Ms751, RoVa, and SiHa cells (Figure 6A). Quantitative analysis showed that the nuclear LNK signal was significantly stronger than the

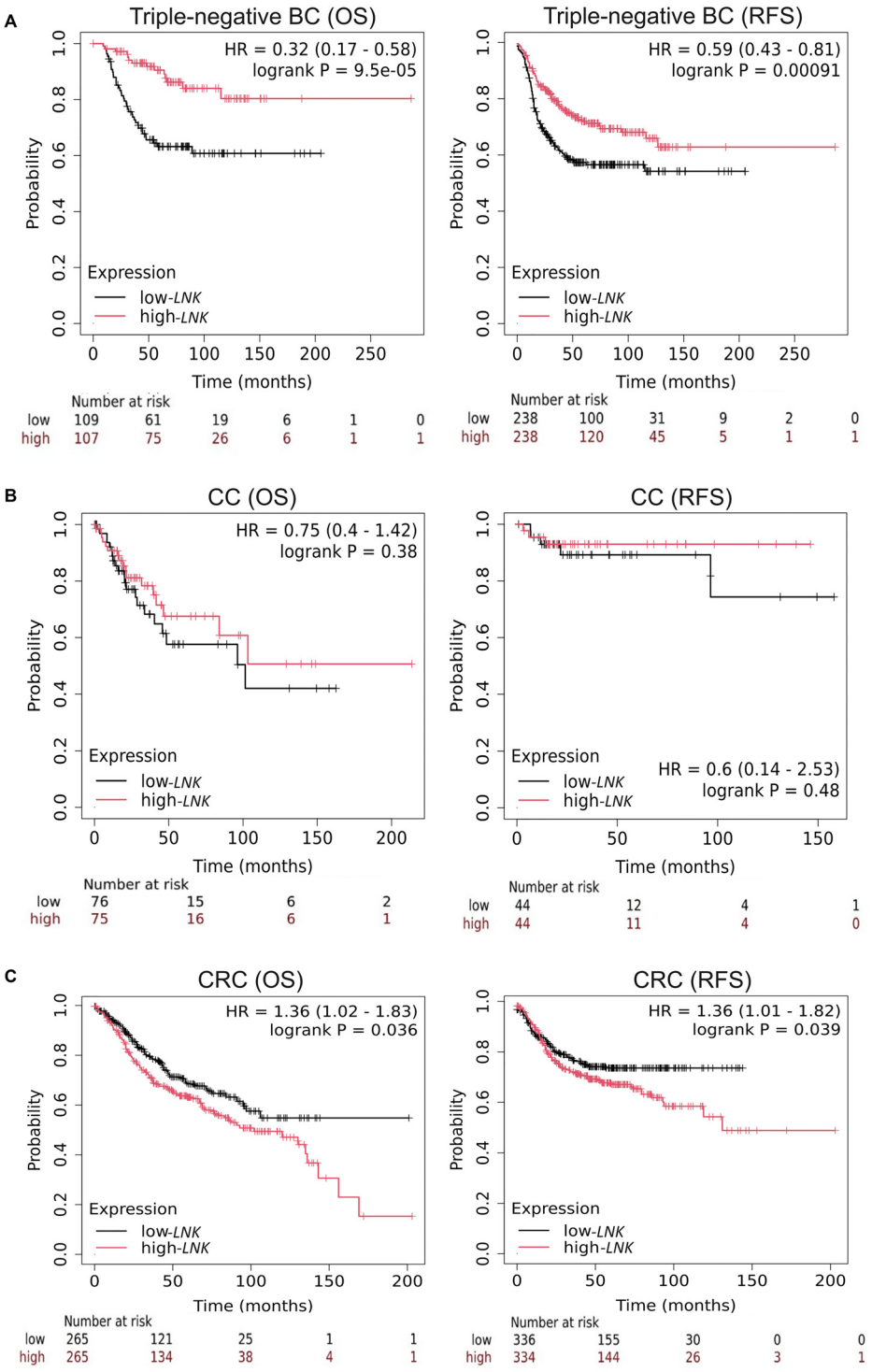



**Figure 3. Association of *LNK* mRNA expression with OS and RFS in triple-negative BC, CC and CRC.** Exploratory survival analyses were performed using KMplot (accessed on 5 July 2025). Kaplan–Meier curves show OS (left) and RFS (right) in patients with (A) triple-negative BC, (B) CC and (C) CRC. Patients in the highest and lowest quartiles of *LNK* mRNA expression were classified as high-*LNK* (red) and low-*LNK* (black), respectively. Tick marks indicate censored observations, and numbers at risk are shown beneath each plot. Follow-up time is expressed in months. Survival curves were compared using the log-rank (Mantel–Cox) test. HRs for high-*LNK* relative to low-*LNK*, with 95% CIs, were estimated using Cox regression and are displayed alongside log-rank *P* values in each plot. No correction for multiple comparisons was applied. High *LNK* expression was associated with longer OS and RFS in triple-negative BC and shorter OS and RFS in CRC, whereas no significant associations were observed in CC. **Abbreviations**: BC, breast cancer; CC, cervical cancer; CI, confidence interval; CRC, colorectal cancer; HR, hazard ratio; KMplot, Kaplan–Meier Plotter; LNK, lymphocyte adaptor protein; mRNA, messenger ribonucleic acid; OS, overall survival; RFS, recurrence-free survival.

**Table 1. Main features of the cell lines studied**

| Cell line | Tumor site/tissue origin | Tumor type | Molecular subtype or virus status | Reference |
|---|---|---|---|---|
| HCC1806 | Breast | Acantholytic squamous cell carcinoma | Basal-like | [36] |
| HCC1937 | Breast | Ductal carcinoma | Basal-like | [37] |
| MDA-MB-231 | Breast | Adenocarcinoma | Basal-like | [38] |
| MDA-MB-468 | Breast | Adenocarcinoma | Basal-like | [39] |
| HeLa | Uterine endocervix | Adenocarcinoma | HPV type 18 | [40] |
| MS751 | Uterine ectocervix | Squamous cell carcinoma | HPV type 18 | [41] |
| RoVa | Uterine ectocervix | Squamous cell carcinoma | HPV type 18 | [29] |
| SiHa | Uterine ectocervix | Squamous cell carcinoma | HPV type 16 | [42] |
| HCT116 | Colon/large intestine | Carcinoma | Microsatellite instability | [43] |
| RKO | Colon/large intestine | Carcinoma | Microsatellite instability | [44] |
| SW480 | Colon/large intestine | Adenocarcinoma | Microsatellite-stable | [45] |
| SW620* | Lymph node | Lymph node metastasis from a primary colorectal adenocarcinoma | Microsatellite-stable | [46] |
| MCF-10A | Mammary gland | Immortalized, non-tumoral | N/A | [47] |
| HaCaT | Epidermal keratinocytes | Immortalized, non-tumoral | N/A | [48] |
| 112CoN | Colon/large intestine | Immortalized, non-tumoral | N/A | [49] |

*: SW620 and SW480, both derived from the same patient, were isolated at different stages of tumor progression. SW620 originated from a metastasis identified later in the disease. **Abbreviations:** HPV, human papillomavirus; N/A, not applicable.

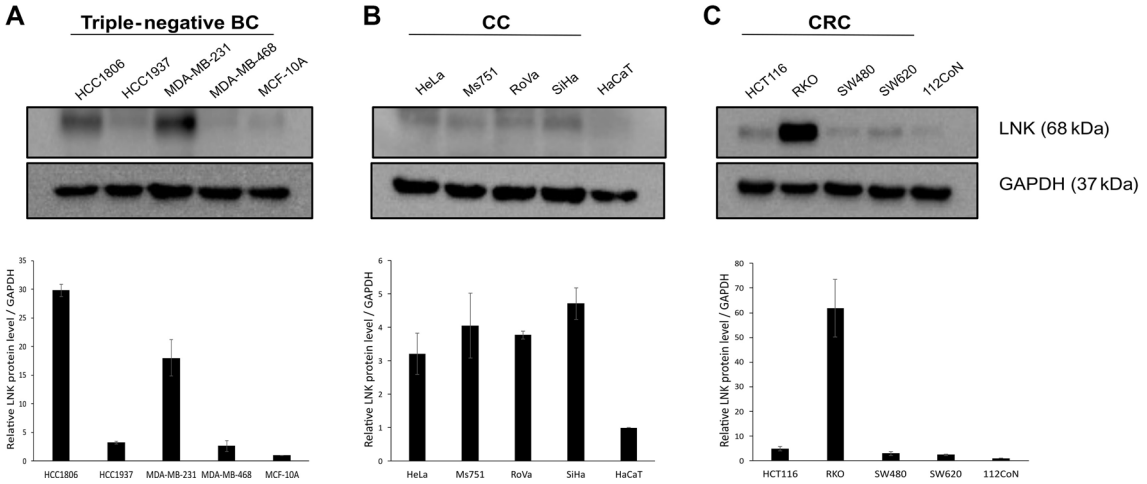



**Figure 4. LNK protein expression in triple-negative BC, CC and CRC cell lines.** Representative Western blots (top) and corresponding densitometric analyses (bottom) are shown for (A) triple-negative BC cell lines HCC1806, HCC1937, MDA-MB-231 and MDA-MB-468, with MCF-10A as the non-tumoral control; (B) CC cell lines HeLa, Ms751, RoVa and SiHa, with HaCaT as the non-tumoral control; and (C) CRC cell lines HCT116, RKO, SW480 and SW620, with 112CoN as the non-tumoral control. LNK was detected at 68 kDa, and GAPDH (37 kDa) served as the loading control. Densitometric values were normalised to GAPDH and expressed as fold change relative to the corresponding non-tumoral control cell line. Bars represent mean ± SEM from two independent experiments. **Abbreviations**: BC, breast cancer; CC, cervical cancer; CRC, colorectal cancer; GAPDH, glyceraldehyde-3-phosphate dehydrogenase; kDa, kilodalton; LNK, lymphocyte adaptor protein; SEM, standard error of the mean.

cytoplasmic signal in the Ms751, RoVa, and SiHa cell lines, but this difference was not significant in HeLa cells. In contrast, the LNK signal was significantly more intense in the cytoplasm compared with the nuclear compartment in the non-tumoral HaCaT cells (Figure 6B).

Unlike BC and CC, CRC cell lines exhibited differential LNK intracellular distributions (Figure 7A). In HCT116 and SW620 cells, the nuclear LNK signal was significantly stronger than the cytoplasmic signal. Conversely, RKO and SW480 showed a clear, significantly stronger LNK signal in the cytoplasmic compartment. The non-tumoral 112CoN cell line displayed a significantly more intense LNK signal in the nucleus than in the cell cytoplasm (Figure 7B).

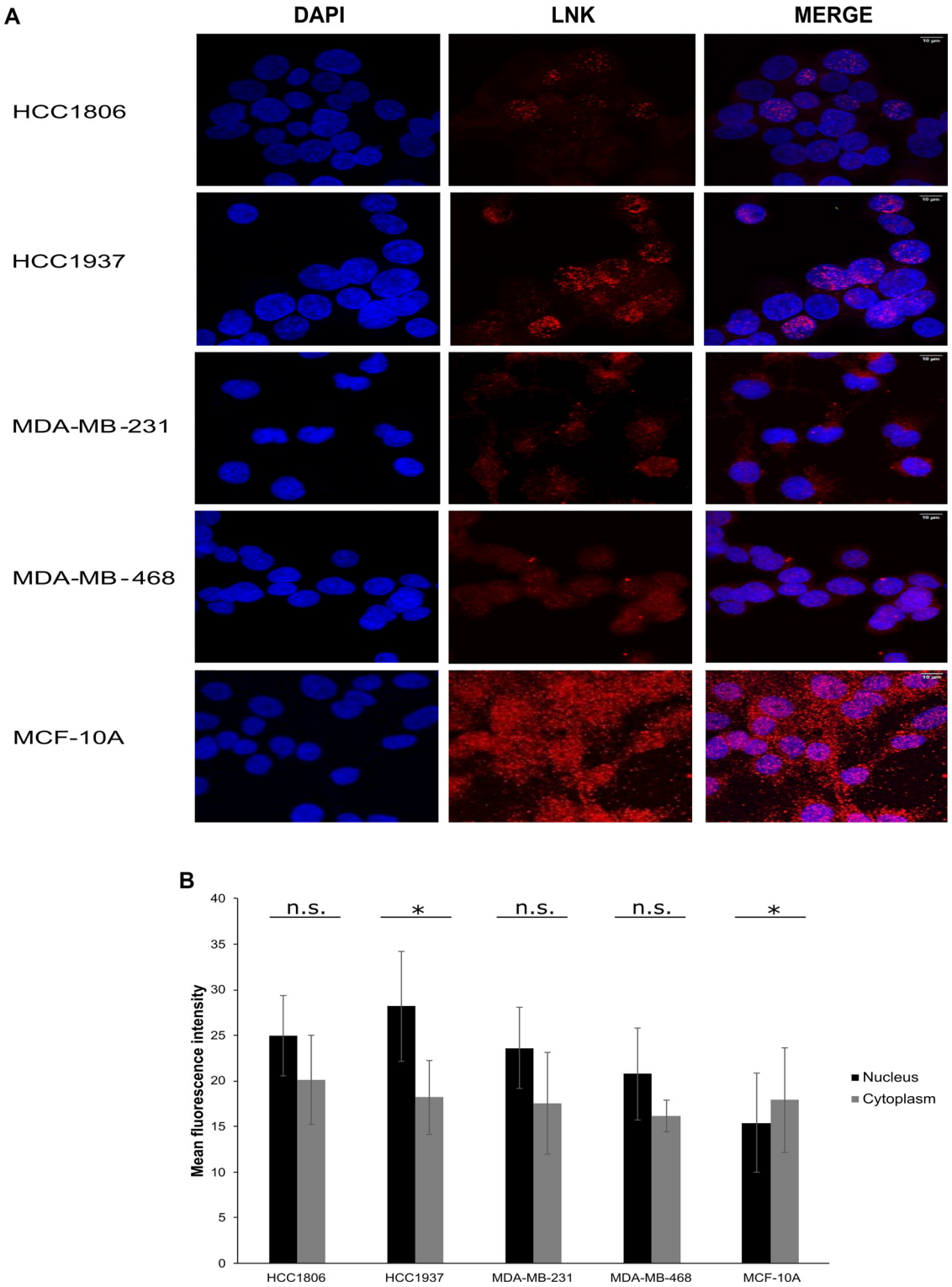



**Figure 5. Intracellular localization of LNK in triple-negative BC cell lines.** (A) Representative confocal immunofluorescence images of HCC1806, HCC1937, MDA-MB-231, MDA-MB-468 and the non-tumoral control MCF-10A. LNK immunostaining is shown in red, nuclei are counterstained with DAPI in blue, and merged images are shown in the right column. (B) Quantitative comparison of LNK fluorescence intensity between the nuclear and cytoplasmic compartments. Bars represent mean fluorescence intensity measured in 20 cells, and error bars indicate SD. Statistical analysis was performed using the aligned rank transform with post hoc Tukey adjustment for multiple comparisons. HCC1937 showed significantly higher nuclear than cytoplasmic LNK signal, whereas MCF-10A showed significantly higher cytoplasmic than nuclear LNK signal. No significant differences between nuclear and cytoplasmic LNK fluorescence intensity were observed in HCC1806, MDA-MB-231 or MDA-MB-468. n.s., not significant; * $P < 0.01$. **Abbreviations**: BC, breast cancer; DAPI, 4′,6-diamidino-2-phenylindole; LNK, lymphocyte adaptor protein; SD, standard deviation.

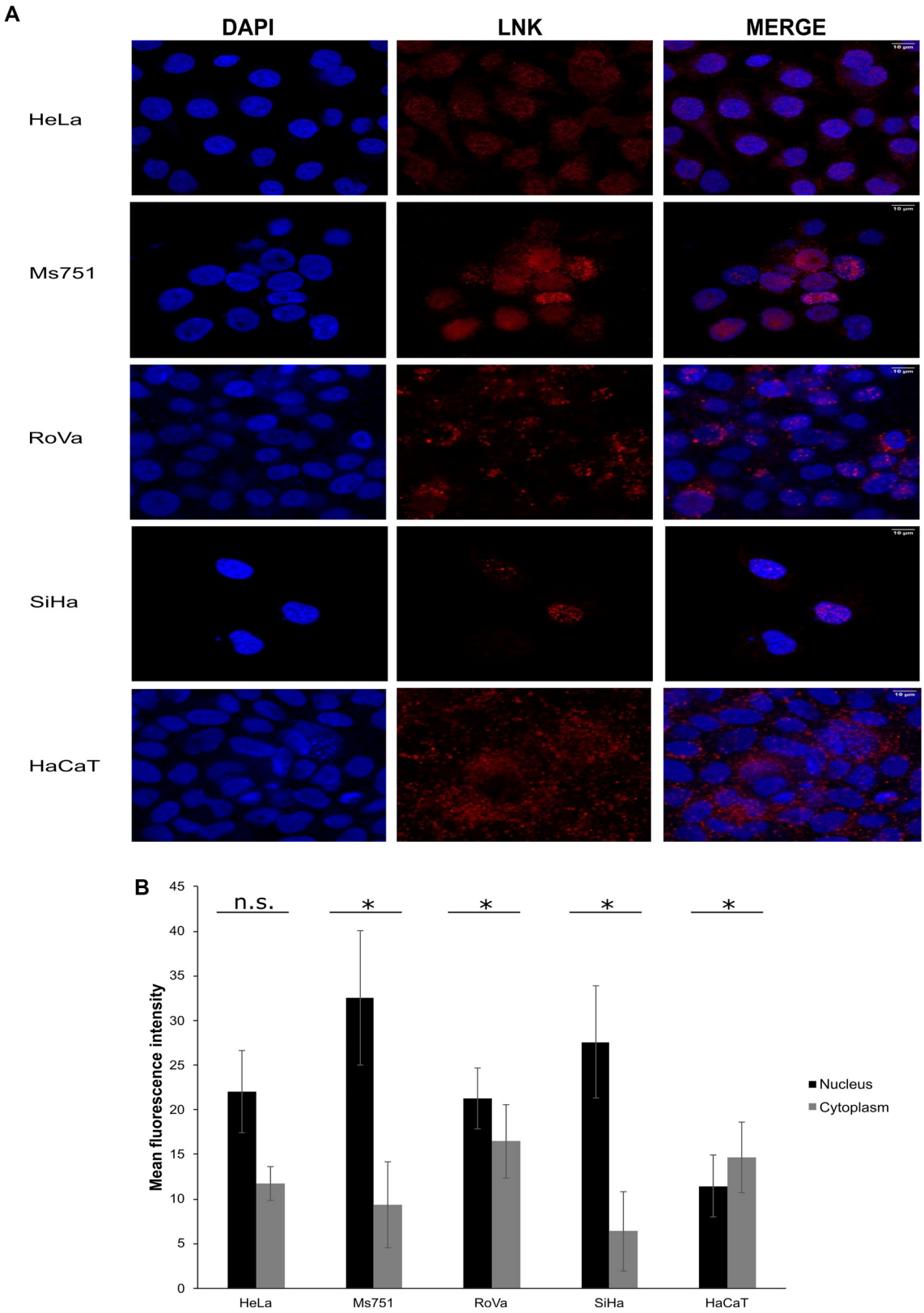



**Figure 6. Intracellular localization of LNK in CC cell lines.** (A) Representative confocal immunofluorescence images of HeLa, Ms751, RoVa, SiHa and the non-tumoral control HaCaT. LNK immunostaining is shown in red, nuclei are counterstained with DAPI in blue, and merged images are shown in the right column. (B) Quantitative comparison of LNK fluorescence intensity between the nuclear and cytoplasmic compartments. Bars represent mean fluorescence intensity measured in 20 cells, and error bars indicate SD. Statistical analysis was performed using the aligned rank transform with post hoc Tukey adjustment for multiple comparisons. Ms751, RoVa and SiHa showed significantly higher nuclear than cytoplasmic LNK signal, whereas HaCaT showed significantly higher cytoplasmic than nuclear LNK signal. No significant difference between nuclear and cytoplasmic LNK fluorescence intensity was observed in HeLa cells. n.s., not significant; * $P < 0.01$. **Abbreviations**: CC, cervical cancer; DAPI, 4′,6-diamidino-2-phenylindole; LNK, lymphocyte adaptor protein; SD, standard deviation.

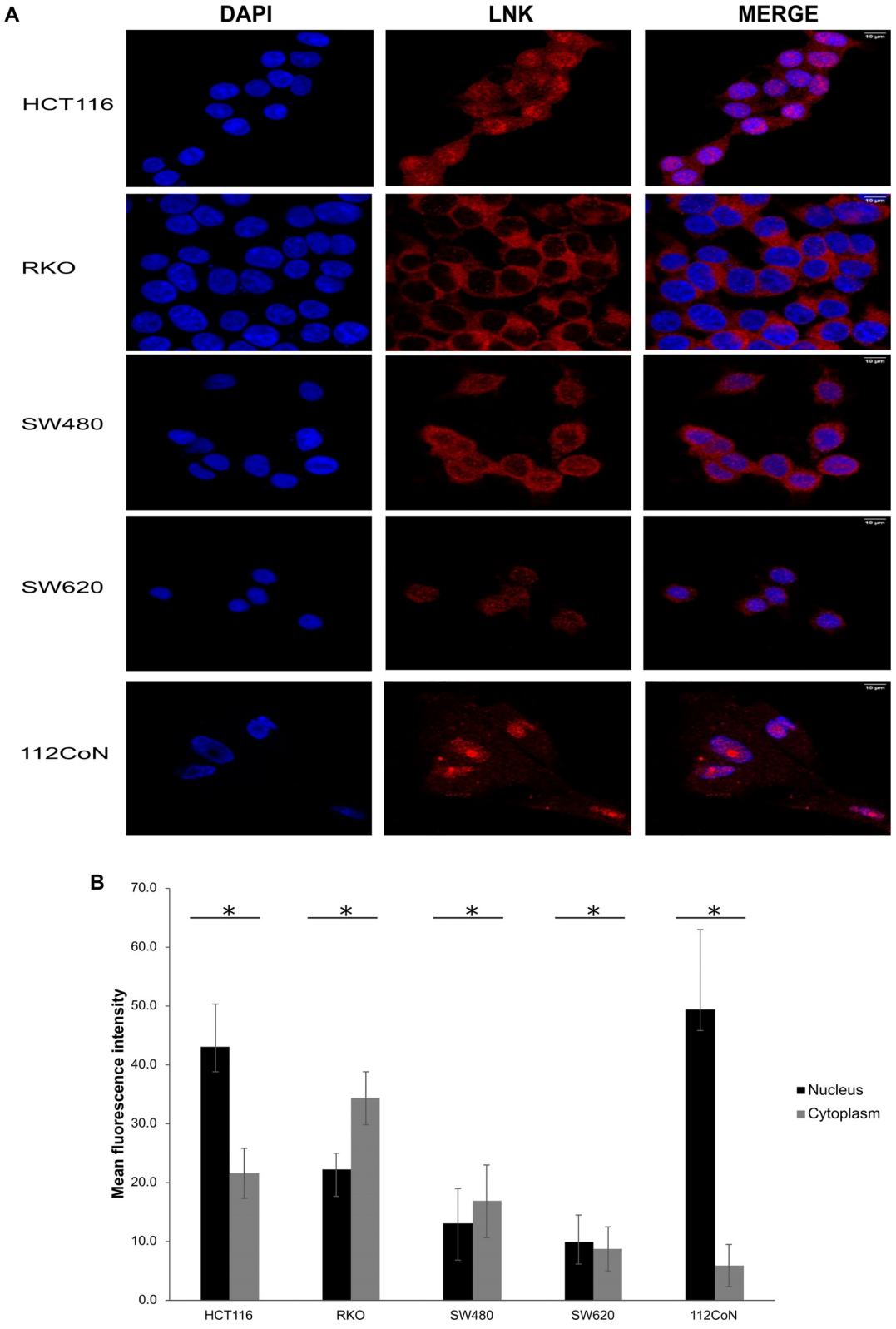



**Figure 7. Intracellular localization of LNK in CRC cell lines.** (A) Representative confocal immunofluorescence images of HCT116, RKO, SW480, SW620 and the non-tumoral control 112CoN. LNK immunostaining is shown in red, nuclei are counterstained with DAPI in blue, and merged images are shown in the right column. (B) Quantitative comparison of LNK fluorescence intensity between the nuclear and cytoplasmic compartments. Bars represent mean fluorescence intensity measured in 20 cells, and error bars indicate SD. Statistical analysis was performed using the aligned rank transform with post hoc Tukey adjustment for multiple comparisons. HCT116, SW620 and 112CoN showed significantly higher nuclear than cytoplasmic LNK signal, whereas RKO and SW480 showed significantly higher cytoplasmic than nuclear LNK signal, indicating heterogeneous intracellular LNK distribution across CRC cell lines. *$P < 0.01$. **Abbreviations**: CRC, colorectal cancer; DAPI, 4′,6-diamidino-2-phenylindole; LNK, lymphocyte adaptor protein; SD, standard deviation.

## Discussion

Functional evidence of LNK expression and gene mutations in hematological disorders has identified LNK as a tumor suppressor in these malignancies. However, LNK's role in solid tumors remains unclear due to limited studies on its expression in this pathological context. In this study, we analyzed LNK expression in human BC, CC, and CRC. Overall, we observed that *LNK* mRNA expression tends to be lower in tumor tissue than in adjacent normal tissue. Similar results were reported in a previous study analyzing *LNK* mRNA and protein expression in 32 CRC samples and matched adjacent normal tissue using reverse transcription–polymerase chain reaction (RT-PCR) and immunohistochemistry [27]. In BC, one study reported significantly higher LNK expression in triple-negative cases than in non-triple-negative cases [22]. Unfortunately, the authors did not compare expression levels with normal breast tissue, making their results incomparable to our data. Regarding CC, our analysis showed significantly lower *LNK* mRNA expression in tumor samples than in adjacent normal tissue. To our knowledge, ours is the first study to report on LNK expression in CC.

Our observations revealed heterogeneous *LNK* mRNA expression across BC, CC, and CRC subtypes. To determine if *LNK* expression is associated with relevant clinical endpoints, we stratified patients by *LNK* mRNA expression level and analyzed OS and RFS. Triple-negative BC patients with high *LNK* mRNA expression showed longer OS and RFS. In a previous study, Lv and colleagues [22] found that triple-negative BC samples exhibited significantly higher LNK levels than other breast tumor subtype samples. However, the authors did not evaluate potential associations between LNK expression and clinical outcomes in their study cohort. Notably, they showed that forced LNK overexpression in a triple-negative BC cell line promoted cell proliferation and migration in a murine xenograft model [22]. This observation appears to contradict our findings; however, experiments using a single genetically modified cell line in an immunosuppressed mouse model may not fully recapitulate physiological conditions observed in patients. Similarly, a more recent report showed that reducing LNK expression via a specific short hairpin RNA (shRNA) targeting *LNK* mRNA in MDA-MB-231 cells decreased cell proliferation, migration, and invasion [50]. Here, we observed that MDA-MB-231 cells express high LNK levels compared with other triple-negative BC cell lines (Figure 4). The MDA-MB-231 cell line was derived from a malignant pleural effusion, a severe complication in patients with advanced, metastatic BC. Furthermore, it has been reported that the MDA-MB-231 cell line comprises distinct cell clusters with different morphodynamic signatures and migratory and invasive capacities, potentially associated with varying transcriptional patterns [51]. Thus, to better evaluate LNK's potential effect in this cancer type, analyzing cell lines representing more clinical stages would be beneficial, as a single cell line may not be representative of this complex pathology.

In contrast to BC, *LNK* mRNA expression in CRC patients negatively correlated with OS and RFS. However, a study of 32 CRC patients reported an association between negative LNK expression and local invasion [27], which contradicts our findings. Our results, based on *LNK* mRNA expression analysis in a dataset of over 500 CRC patients, are not directly comparable to their immunohistochemistry data, which classified samples as LNK-positive or LNK-negative. To establish LNK's value as a clinical outcome biomarker, further studies on LNK protein expression in a larger number of tumor biopsies are essential.

For CC patients, we found no association between *LNK* mRNA expression and clinical responses. This is the first study to report LNK expression in CC patients, suggesting that LNK expression in cancer may be tissue-specific and potentially linked to clinical outcomes. However, validating these observations requires analyzing larger databases and experimental confirmation.

Our study revealed that *LNK* mRNA expression tended to be lower in tumors than in adjacent normal tissue. This contrasts with LNK protein levels detected in cell lines and their non-tumoral counterparts. It is important to note that immortalized cell lines may not fully replicate the genetic and molecular characteristics of normal cells. Consistent with our findings, previous research shows that immortalized cell lines can exhibit different protein [52] and microRNA [53] expression profiles compared to normal adjacent tissues.

The intracellular localization of LNK across human tissues and cell lines has not been specifically examined. Consulting The Human Protein Atlas (https://www.proteinatlas.org), we observed highly heterogeneous LNK subcellular localization, even in normal tissue [54]. For example, LNK immunostaining was cytoplasmic and membranous in liver and kidney cells but exclusively nuclear in lymph node and skin cells. In BC, immunofluorescence showed nuclear LNK localization in the BC-derived MCF-7 cell line [54], consistent with our results. However, immunohistochemistry in BC tissue slides revealed LNK in the cytoplasm, both cytoplasm and membranous compartments, or exclusively in the nucleus, likely due to the inclusion of different molecular subtypes. Strikingly, CRC tissue slides showed only nuclear LNK staining, while normal colon cells exhibited cytoplasmic, membranous, and nuclear positivity. In CC samples, LNK immunostaining was observed in the cytoplasm and nucleus. The presence of cells with exclusively nuclear LNK and others with cytoplasmic and nuclear immunostaining on the same tissue slide suggests that LNK localization may be both tissue-specific and dependent on tumor-intrinsic heterogeneity. The biological significance of intracellular LNK location remains unexplored. Notably, LNK is nuclear in preleptotene spermatocytes but cytoplasmic and membranous in early and late spermatids [54], suggesting a dynamic function potentially associated with differentiation.

The role of LNK in solid tumors is not fully understood. This report provides insights into this regulatory molecule in BC, CC, and CRC. However, this exploratory analysis has limitations. While we used various tumor cell lines and non-tumoral controls to determine LNK expression and intracellular localization, HaCaT are human keratinocytes and 112CoN are colon fibroblasts; thus, tissue-matched control cell

lines would be more appropriate for comparison with CC and CRC tumor-derived cells. Additionally, we did not validate our observations by evaluating LNK localization in tumor tissue samples. Another limitation is the lack of functional experiments to assess LNK's impact on cancer-associated activities like proliferation, chemoresistance, and survival, and to investigate its potential nuclear functions. Such experiments would help elucidate LNK's activities in solid tumors. Finally, survival analyses were performed using the KMplot platform, which stratifies patients based on expression-based cutoffs without adjusting for important clinical confounders. Therefore, these findings are exploratory and hypothesis-generating; independent multivariable analyses in well-annotated cohorts are necessary for validation.

## Conclusion

Transcriptomic data revealed that *LNK* mRNA expression and its impact on clinical outcomes varied across tumor types, suggesting that LNK may be a tissue- and/or cancer type-specific molecule.

At the cellular level, we demonstrated LNK's presence in the nuclear-cytoplasmic compartment of the examined tumor cell lines. The detection of LNK in the cell nucleus is particularly intriguing, as there is currently no evidence for its potential nuclear function, thus opening a new area of research for this regulatory molecule.

## Acknowledgments

Jessica C. Mantilla-Ollarves, a student in the Programa de Doctorado en Ciencias Bioquímicas at the Universidad Nacional Autónoma de México (UNAM), received fellowship number 1012524 from the Secretaría de Ciencia, Humanidades, Tecnología e Innovación (SECIHTI). The authors thank Lucía B. Brito Ocampo for technical assistance.

**Conflicts of interest:** Authors declare no conflicts of interest.

**Funding:** This research was funded by grants from PAPIIT, Universidad Nacional Autónoma de México (IN206022) and (IN202625) and by the Programa Institucional de Cáncer de Mama, Instituto de Investigaciones Biomédicas, UNAM.

**Data availability:** The data supporting the study findings of this study are available upon request from the corresponding author.

Submitted: 17 April 2026
Accepted: 29 July 2026
Published online: 17 September 2026

## References

[1] Sung H, Filho AM, Laversanne M, Ferlay J, Siegel RL, Soerjomataram I, et al. Global cancer statistics 2024:GLOBOCAN estimates of incidence and mortality worldwide for 34 cancers in 186 countries. CA Cancer J Clin 2026;76(4):e70090. https://doi.org/10.3322/caac.70090.

[2] Leon-Ferre RA, Goetz MP. Advances in systemic therapies for triple negative breast cancer. BMJ 2023;381:e071674. https://doi.org/10.1136/bmj-2022-071674.

[3] Naga CH P, Gurram L, Chopra S, Mahantshetty U. The management of locally advanced cervical cancer. Curr Opin Oncol 2018;30(5):323–9. https://doi.org/10.1097/CCO.0000000000000471.

[4] Biller LH, Schrag D. Diagnosis and treatment of metastatic colorectal cancer: a review. JAMA 2021;325(7):669–85. https://doi.org/10.1001/jama.2021.0106.

[5] Pan L, Chen X, Rassool FV, Li C, Lin J. LLL12B, a novel small-molecule STAT3 inhibitor, induces apoptosis and suppresses cell migration and tumor growth in triple-negative breast cancer cells. Biomedicines 2022;10(8):2003. https://doi.org/10.3390/biomedicines10082003.

[6] Kruger DT, Opdam M, Sanders J, van der Noort V, Boven E, Linn SC. Hierarchical clustering of PI3K and MAPK pathway proteins in breast cancer intrinsic subtypes. APMIS 2020;128(4):298–307. https://doi.org/10.1111/apm.13026.

[7] Erdogan F, Radu TB, Orlova A, Qadree AK, de Araujo ED, Israelian J, et al. JAK-STAT core cancer pathway: an integrative cancer interactome analysis. J Cell Mol Med 2022;26(7):2049–62. https://doi.org/10.1111/jcmm.17228.

[8] Hashemi M, Abbaszadeh S, Rashidi M, Amini N, Talebi Anaraki K, Motahhary M, et al. STAT3 as a newly emerging target in colorectal cancer therapy: tumorigenesis, therapy response, and pharmacological/nanoplatform strategies. Environ Res 2023;233:116458. https://doi.org/10.1016/j.envres.2023.116458.

[9] Leiphrakpam PD, Are C. PI3K/Akt/mTOR signaling pathway as a target for colorectal cancer treatment. Int J Mol Sci 2024;25(6):3178. https://doi.org/10.3390/ijms25063178.

[10] Fang JY, Richardson BC. The MAPK signalling pathways and colorectal cancer. Lancet Oncol 2005;6(5):322–7. https://doi.org/10.1016/S1470-2045(05)70168-6.

[11] Lopez TV, Lappin TRJ, Maxwell P, Shi Z, Lopez-Marure R, Aguilar C, et al. Autocrine/paracrine erythropoietin signalling promotes JAK/STAT-dependent proliferation of human cervical cancer cells. Int J Cancer 2011;129(11):2566–76. https://doi.org/10.1002/ijc.25935.

[12] Vázquez-Mellado MJ, Cortés-Ballinas LG, Blanco-Flores IC, Aguilar C, Vázquez-Gómez G, Rocha-Zavaleta L. Erythropoietin promotes expression of survivin via STAT3 activation and reduces sensitivity to cisplatin in cervical cancer cells. Oncol Rep 2019;41(2):1333–41. https://doi.org/10.3892/or.2018.6890.

[13] Zhang T, Xiaohan C. Unveiling the role of JAK2/STAT3 signaling in chemoresistance of gynecological cancers: from mechanisms to therapeutic implications. Crit Rev Oncol Hematol 2025;211:104712. https://doi.org/10.1016/j.critrevonc.2025.104712.

[14] Bossler F, Hoppe-Seyler K, Hoppe-Seyler F. PI3K/AKT/mTOR signaling regulates the virus/host cell crosstalk in HPV-positive cervical cancer cells. Int J Mol Sci 2019;20(9):2188. https://doi.org/10.3390/ijms20092188.

[15] Rasi Bonab F, Baghbanzadeh A, Ghaseminia M, Bolandi N, Mokhtarzadeh A, Amini M, et al. Molecular pathways in the development of HPV-induced cervical cancer. EXCLI J 2021;20:320–37. https://doi.org/10.17179/excli2021-3365.

[16] Tong W, Lodish HF. Lnk inhibits Tpo-mpl signaling and Tpo-mediated megakaryocytopoiesis. J Exp Med 2004;200(5):569–80. https://doi.org/10.1084/jem.20040762.

[17] Tong W, Zhang J, Lodish HF. Lnk inhibits erythropoiesis and Epo-dependent JAK2 activation and downstream signaling pathways. Blood 2005;105(12):4604–12. https://doi.org/10.1182/blood-2004-10-4093.

[18] Li Y, He X, Schembri-King J, Jakes S, Hayashi J. Cloning and characterization of human Lnk, an adaptor protein with pleckstrin homology and Src homology 2 domains that can inhibit T cell activation. J Immunol 2000;164(10):5199–206. https://doi.org/10.4049/jimmunol.164.10.5199.

[19] Harlan JE, Hajduk PJ, Yoon HS, Fesik SW. Pleckstrin homology domains bind to phosphatidylinositol-4,5-bisphosphate. Nature 1994;371(6493):168–70. https://doi.org/10.1038/371168a0.

[20] Maslah N, Cassinat B, Verger E, Kiladjian JJ, Velazquez L. The role of LNK/SH2B3 genetic alterations in myeloproliferative neoplasms and other hematological disorders. Leukemia 2017;31(8):1661–70. https://doi.org/10.1038/leu.2017.139.

[21] Meyer SC, Levine RL. Molecular pathways: molecular basis for sensitivity and resistance to JAK kinase inhibitors. Clin Cancer Res 2014;20(8):2051–9. https://doi.org/10.1158/1078-0432.CCR-13-0279.

[22] Lv J, Yu W, Zhang Y, Cao X, Han L, Hu H, et al. LNK promotes the growth and metastasis of triple negative breast cancer via activating JAK/STAT3 and ERK1/2 pathway. Cancer Cell Int 2020;20:124. https://doi.org/10.1186/s12935-020-01197-9.

[23] Ding LW, Sun QY, Lin DC, Chien W, Hattori N, Dong XM, et al. LNK (SH2B3): paradoxical effects in ovarian cancer. Oncogene 2015;34(11):1463–74. https://doi.org/10.1038/onc.2014.34.
[24] Zhong ZM, Chen X, Qi X, Wang XM, Li CY, Qin RJ, et al. Adaptor protein LNK promotes anaplastic thyroid carcinoma cell growth via 14-3-3. $\epsilon/\gamma$ binding. Cancer Cell Int 2020;20:11. https://doi.org/10.1186/s12935-019-1090-9
[25] Cai S, Lu JX, Wang YP, Shi CJ, Yuan T, Wang X-P. SH2B3, transcribed by STAT1, promotes glioblastoma progression through transducing IL-6/gp130 signaling to activate STAT3 signaling. Front Cell Dev Biol 2021;9:606527. https://doi.org/10.3389/fcell.2021.606527.
[26] Ding LW, Sun QY, Edwards JJ, Fernández LT, Ran XB, Zhou SQ, et al. LNK suppresses interferon signaling in melanoma. Nat Commun 2019;10(1):2230. https://doi.org/10.1038/s41467-019-09711-y.
[27] Pan J, Peng R, Cheng N, Chen F, Gao B. LNK protein: low expression in human colorectal carcinoma and relationship with tumor invasion. Biomed Pharmacother 2020;121:109467. https://doi.org/10.1016/j.biopha.2019.109467.
[28] Wang LN, Zhang ZT, Wang L, Wei HX, Zhang T, Zhang LM, et al. TGF-β1/SH2B3 axis regulates anoikis resistance and EMT of lung cancer cells by modulating JAK2/STAT3 and SHP2/Grb2 signaling pathways. Cell Death Dis 2022;13(5):472. https://doi.org/10.1038/s41419-022-04890-x.
[29] Hidalgo A, Monroy A, Arana RM, Taja L, Vázquez G, Salcedo M. Chromosomal imbalances in four new uterine cervix carcinoma derived cell lines. BMC Cancer 2003;3:8. https://doi.org/10.1186/1471-2407-3-8.
[30] Schindelin J, Arganda-Carreras I, Frise E, Kaynig V, Longair M, Pietzsch T, et al. Fiji: an open-source platform for biological-image analysis. Nat Methods 2012;9(7):676–82. https://doi.org/10.1038/nmeth.2019
[31] Tang Z, Kang B, Li C, Chen T, Zhang Z. GEPIA2:an enhanced web server for large-scale expression profiling and interactive analysis. Nucleic Acids Res 2019;47(W1):W556–W560. https://doi.org/10.1093/nar/gkz430.
[32] Cancer Genome Atlas Research Network,Weinstein JN, Collison EA, Mills GB, Mills Shaw KR, Ozenberger BA, et al. The Cancer Genome Atlas pan-cancer analysis project. Nat Genet 2013;45(10):1113–20. https://doi.org/10.1038/ng.2764
[33] Lánczky A, Győrffy B. Web-based survival analysis tool tailored for medical research (KMplot): development and implementation. J Med Internet Res 2021;23(7):e27633. https://doi.org/10.2196/27633.
[34] Győrffy B, Lanczky A, Eklund AC, Denkert C, Budczies J, Li Q, et al. An online survival analysis tool to rapidly assess the effect of 22,277 genes on breast cancer prognosis using microarray data of 1,809 patients. Breast Cancer Res Treat 2010;123(3):725–31. https://doi.org/10.1007/s10549-009-0674-9.
[35] Mihály Z, Kormos M, Lánczky A, Dank M, Budczies J, Szász MA, et al. A meta-analysis of gene expression-based biomarkers predicting outcome after tamoxifen treatment in breast cancer. Breast Cancer Res Treat 2013;140(2):219–32. https://doi.org/10.1007/s10549-013-2622-y.
[36] American Type Culture Collection (ATCC). HCC1806 (ATCC® CRL-2335) [Internet]. Manassas (VA): ATCC; [cited 2026 Jul 14]. Available from: https://www.atcc.org/products/crl-2335
[37] American Type Culture Collection (ATCC). HCC1937 (ATCC® CRL-2336) [Internet]. Manassas (VA): ATCC; [cited 2026 Jul 12]. Available from: https://www.atcc.org/products/crl-2336
[38] American Type Culture Collection (ATCC). MDA-MB-231 (ATCC® CRM-HTB-26) [Internet]. Manassas (VA): ATCC; [cited 2026 Jul 12]. Available from: https://www.atcc.org/products/crm-htb-26
[39] American Type Culture Collection (ATCC). MDA-MB-468 (ATCC® HTB-132) [Internet]. Manassas (VA): ATCC; [cited 2026 Jul 12]. Available from: https://www.atcc.org/products/htb-132
[40] American Type Culture Collection (ATCC). HeLa (ATCC® CRM-CCL-2) [Internet]. Manassas (VA): ATCC; [cited 2026 Jul 12]. Available from: https://www.atcc.org/products/crm-ccl-2
[41] American Type Culture Collection (ATCC). Ms751 (ATCC® HTB-34) [Internet]. Manassas (VA): ATCC; [cited 2026 Jul 12]. Available from: https://www.atcc.org/products/htb-34
[42] American Type Culture Collection (ATCC). SiHa (ATCC® HTB-35) [Internet]. Manassas (VA): ATCC; [cited 2026 Jul 12]. Available from: https://www.atcc.org/products/htb-35
[43] American Type Culture Collection (ATCC). HCT116 (ATCC® CCL-247EMT) [Internet]. Manassas (VA): ATCC; [cited 2026 Jul 12]. Available from: https://www.atcc.org/products/ccl-247emt
[44] American Type Culture Collection (ATCC). RKO (ATCC® CCL-247EMT) [Internet]. Manassas (VA): ATCC; [cited 2026 Jul 12]. Available from: https://www.atcc.org/products/crl-2577
[45] American Type Culture Collection (ATCC). SW480 (ATCC® CCL-228) [Internet]. Manassas (VA): ATCC; [cited 2026 Jul 12]. Available from: https://www.atcc.org/products/ccl-228
[46] American Type Culture Collection (ATCC). SW620 (ATCC® CCL-227) [Internet]. Manassas (VA): ATCC; [cited 2026 Jul 12]. Available from: https://www.atcc.org/products/ccl-227
[47] American Type Culture Collection (ATCC). MCF 10A (ATCC® CRL-10317) [Internet]. Manassas (VA): ATCC; [cited 2026 Jul 12]. Available from: https://www.atcc.org/products/crl-10317
[48] Cytion GmbH. HaCaT cells [Internet]. Alemania: Cytion GmbH; [cited 2026 Jul 12]. Available from: https://www.cytion.com/HaCaT-Cells/300493
[49] American Type Culture Collection (ATCC). CCD-112CoN (ATCC® CRL-1541) [Internet]. Manassas (VA): ATCC; [cited 2026 Jul 12]. Available from: https://www.atcc.org/products/crl-1541
[50] Shi X, Hao R, Yang Z, Wang X, Lu Y, Wang X, et al. KAT2A-H3K79succ-mediated SH2B3 upregulation promotes TNBC metastasis through diminishing the ubiquitin-dependent degradation of vimentin. FASEB J 2025;39(20):e71140. https://doi.org/10.1096/fj.202502178R.
[51] Zhang X, Chan T, Mak M. Morphodynamic signatures of MDA-MB-231 single cells and cell doublets undergoing invasion in confined microenvironments. Sci Rep 2021;11(1):6529. https://doi.org/10.1038/s41598-021-85640-5.
[52] Feng X, Lin J, Xing S, Liu W, Zhang G. Higher IGFBP-1 to IGF-1 serum ratio predicts unfavourable survival in patients with nasopharyngeal carcinoma. BMC Cancer 2017;17(1):90. https://doi.org/10.1186/s12885-017-3068-0.
[53] McCall MN, Kim MS, Adil M, Patil AH, Lu Y, Mitchell CJ, et al. Toward the human cellular microRNAome. Genome Res 2017;27(10):1769–81. https://doi.org/10.1101/gr.222067.117
[54] Uhlén M, Fagerberg L, Hallström BM, Lindskog C, Oksvold P, Mardinoglu A, et al. Tissue-based map of the human proteome. Science 2015;347(6220):1260419. https://doi.org/10.1126/science.1260419.

## Related articles

1. The prognostic value of MKL1 in predicting breast cancer immune infiltrates and chemosensitivity

Yijia Hua and Mengzhu Yang, BJBMS, 2021

2. LncRNA interactomes and co-methylation in breast cancer regulation

Elena A. Filippova et al., Biomol Biomed, 2025

3. A preliminary study on the prognostic significance of cysteine-rich EGF ligand domain 2 protein (CRELD2) in patients with triple negative breast cancer

Mehmet Zahid Koçak et al., Biomol Biomed, 2025